Supporting Materials for paper

Mechanosynthesis of cocrystals and coamorphous binary drug–drug systems with apremilast core: structural and biological studies

K. Trzeciak[1], R. Dolot[1], M. K. Dudek[1], E. Wielgus[1], S. Kazmierski[1], P. Paluch[1], J. Czernek[2], J. Brus[2], K. Wiktorska[3], I. Wadas[3], K. Głowacka[3,4], A. Lange[3], and M. J Potrzebowski[1]*

1) Centre of Molecular and Macromolecular Studies, Polish Academy of Sciences, Sienkiewicza 112, 90-363 Łódź, Poland.
2) Institute of Macromolecular Chemistry, Czech Academy of Sciences, Heyrovského nám. 1888/2, Prague 6, Czech Republic
3) Institute of Biology Warsaw, University of Life Sciences-SGGW, , Nowoursynowska 159, 02-787 Warsaw, Poland
4) Department of Chemistry, University of Warsaw, Pasteura 1, 02-093 Warszawa, Poland

Content

1) X-ray crystal structures of coformers SA, ET, and PA.

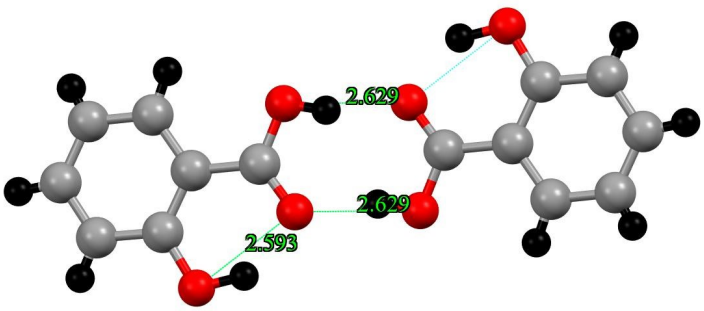

Figure S1a. Hydrogen bond distances in angstroms (green color) in the crystal lattice of salicylic acid. The structure was drawn using X-ray data deposited in the CCDC under the code SALIAC01.

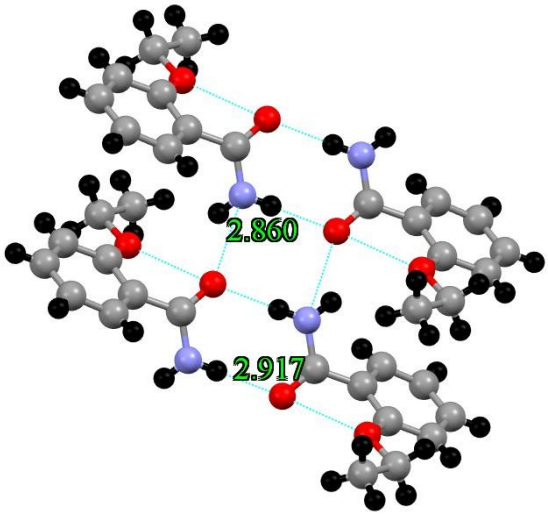

Figure S1b. Hydrogen bond distances in angstroms (green color) in the crystal lattice of ethenzamide. The structure was drawn using X-ray data deposited in the CCDC under the code DUKXAJ.

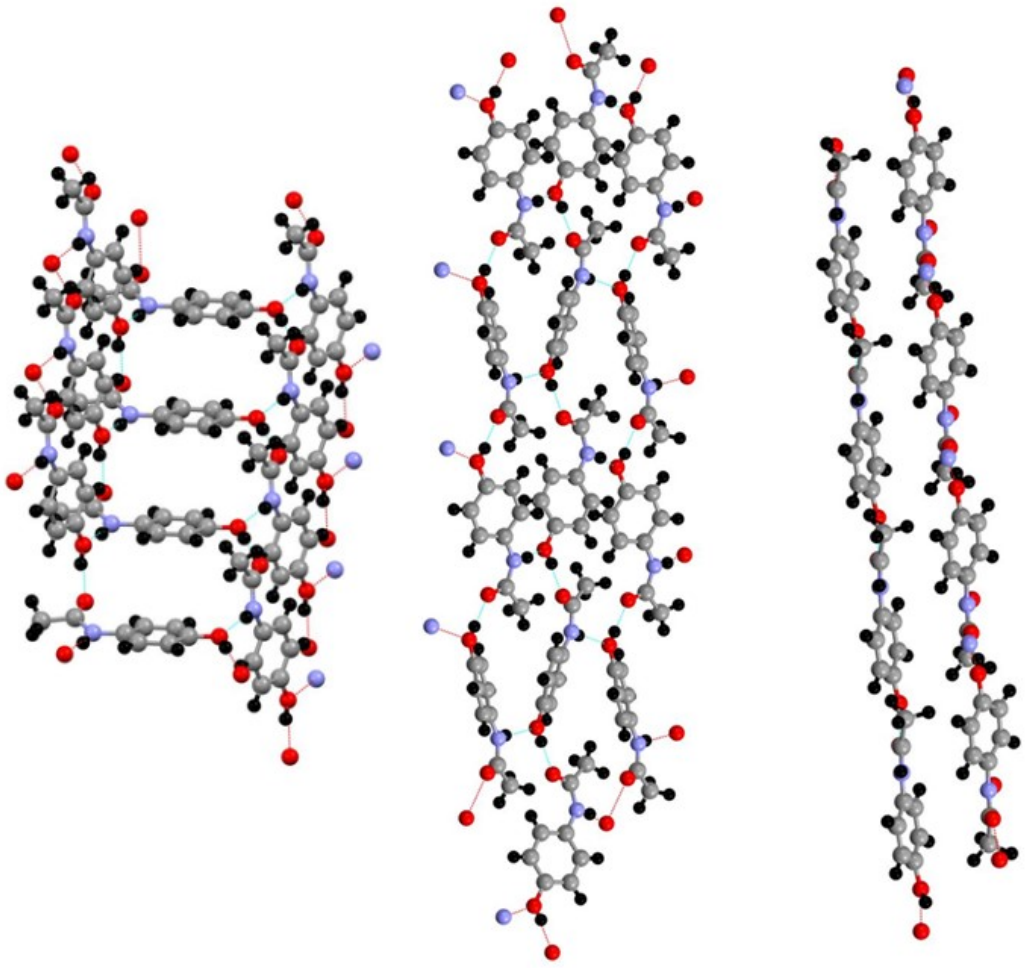

Figure S1c. Polymorphic structures of paracetamol. On the left, Polymorph I (reference code CCDC HXACAN01), in the center, Polymorph II (reference code CCDC HXACAN23), and on the right, Polymorph III (CCDC deposit numbers 716555)

2) ^{1}H Very Fast MAS NMR.

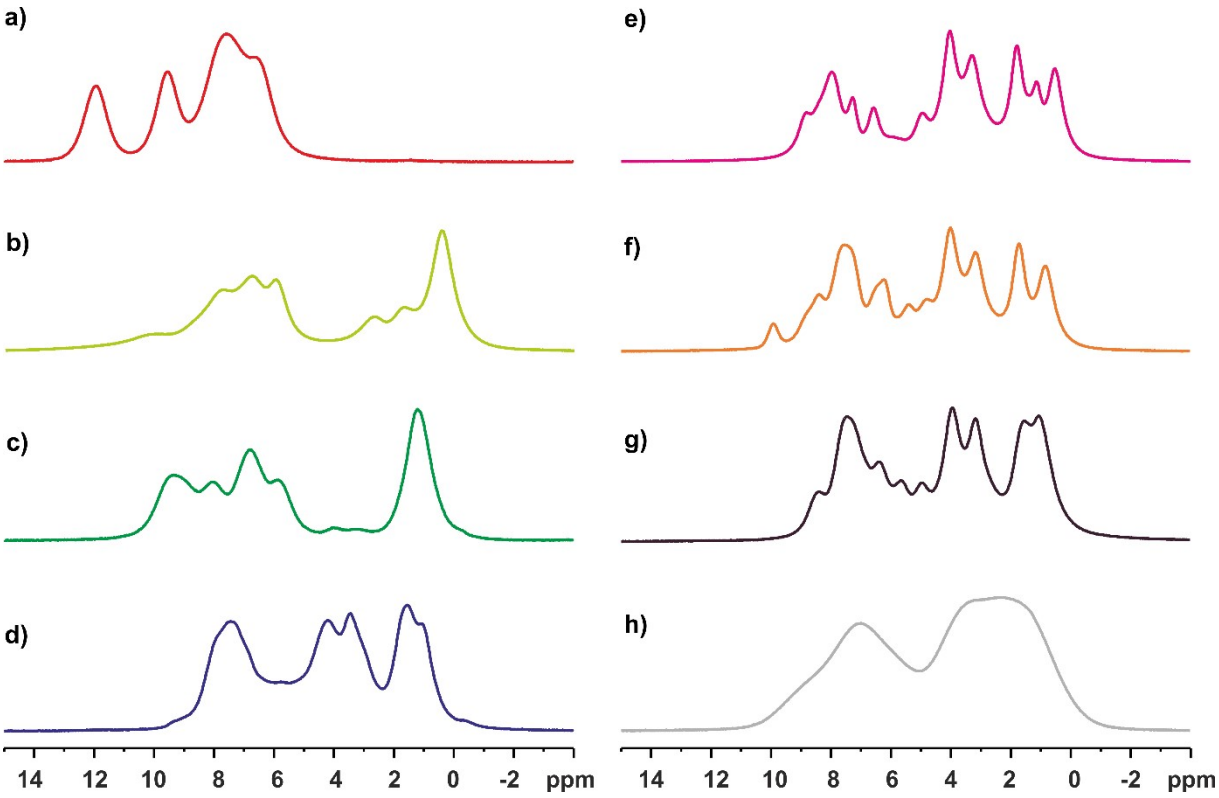

Figure S2. ^{1}H VF MAS NMR spectra of: (a) SA, (b) ET, (c) PA, (d) APR(B), (e) APR(E), (f) APR:SA, (g) APR:ET, and (h) APR(E):PA after thermal grinding, recorded at a spinning rate of 50 kHz.

3) Powder X-ray Diffraction data, Experimental and Calculated Diffractograms.

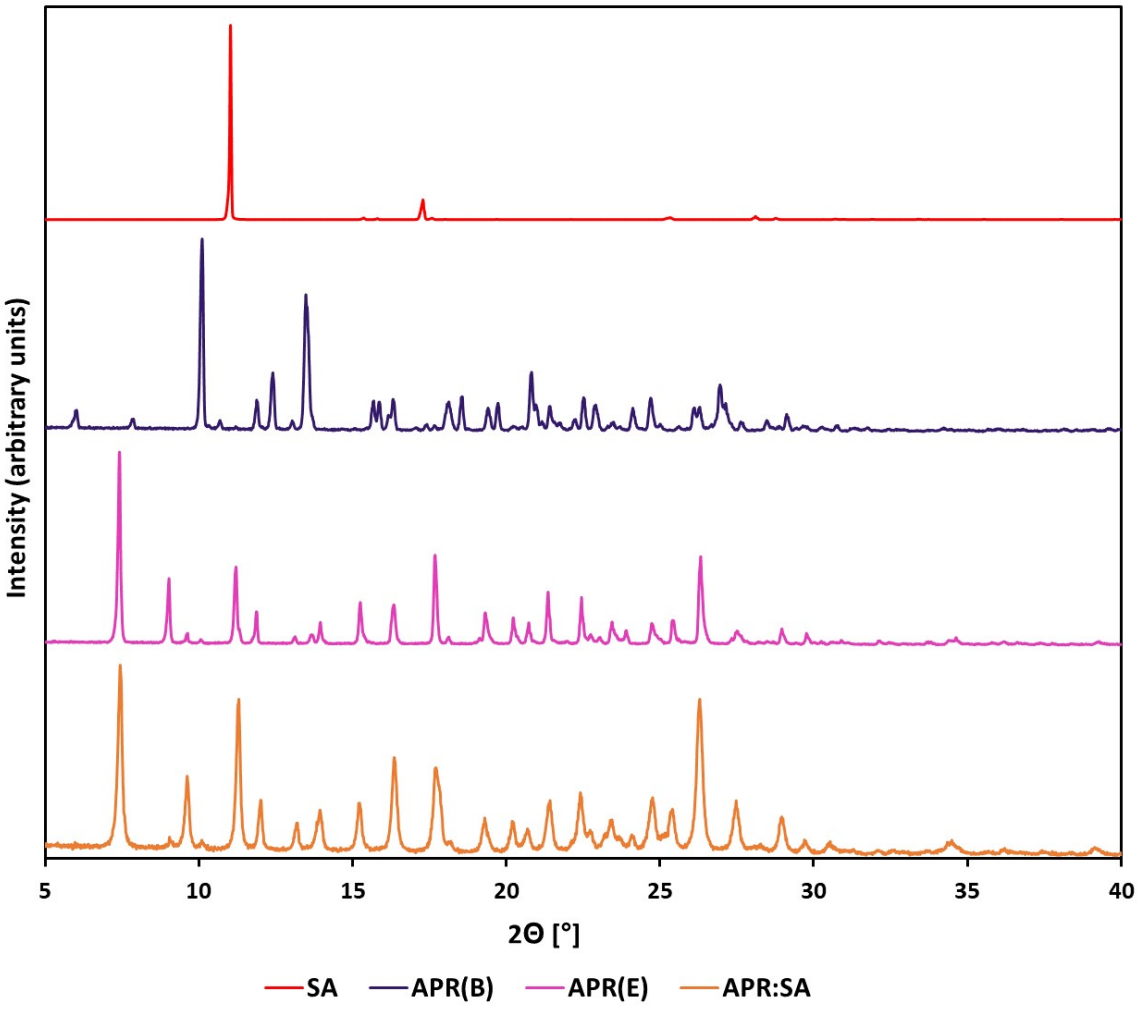

Figure S3a. Normalised PXRD patterns of pure SA, APR(B), APR(E), and the APR:SA cocrystal.

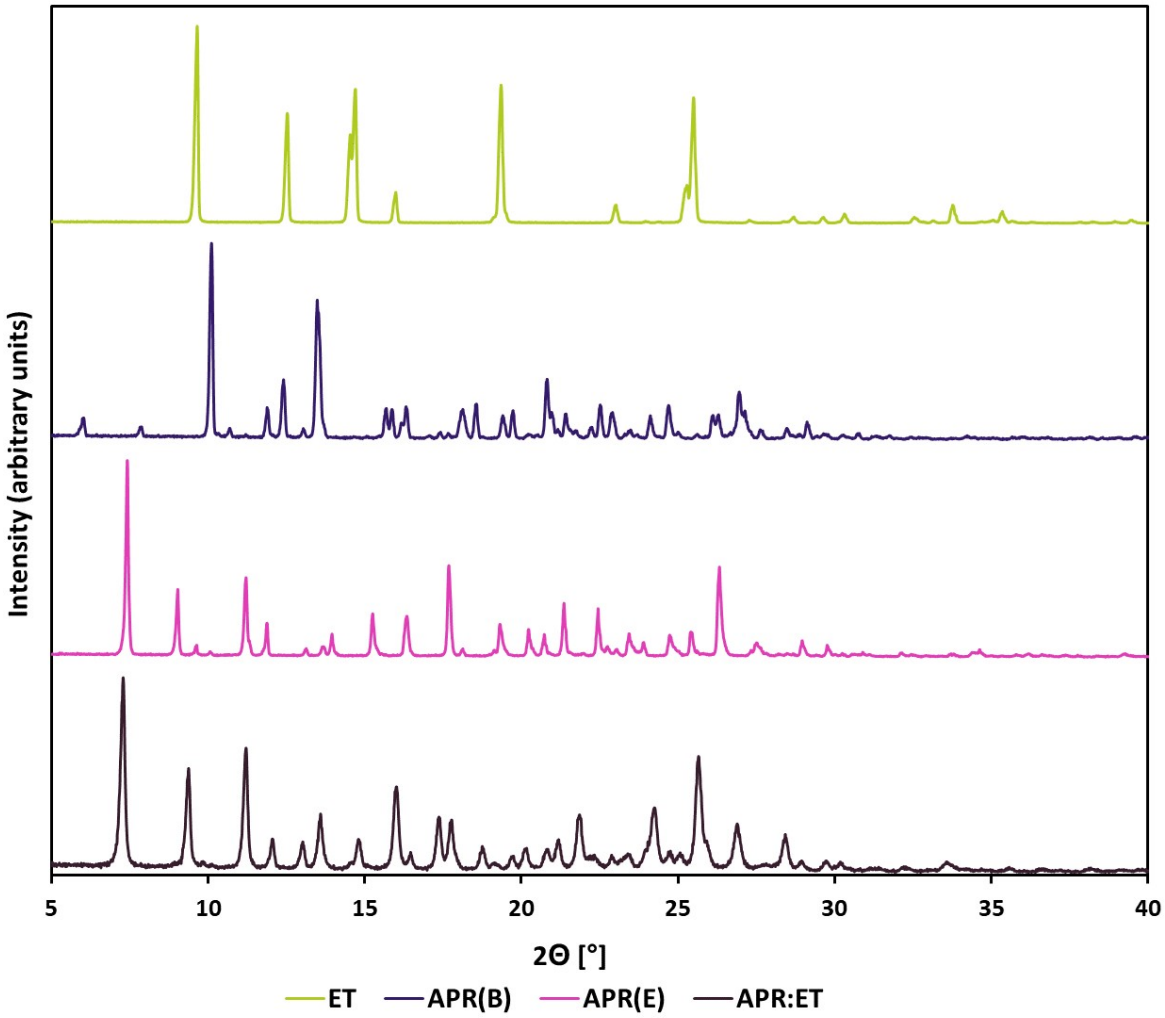

Figure S3b. Normalised PXRD patterns of pure ET, APR(B), APR(E), and the APR:ET cocrystal.

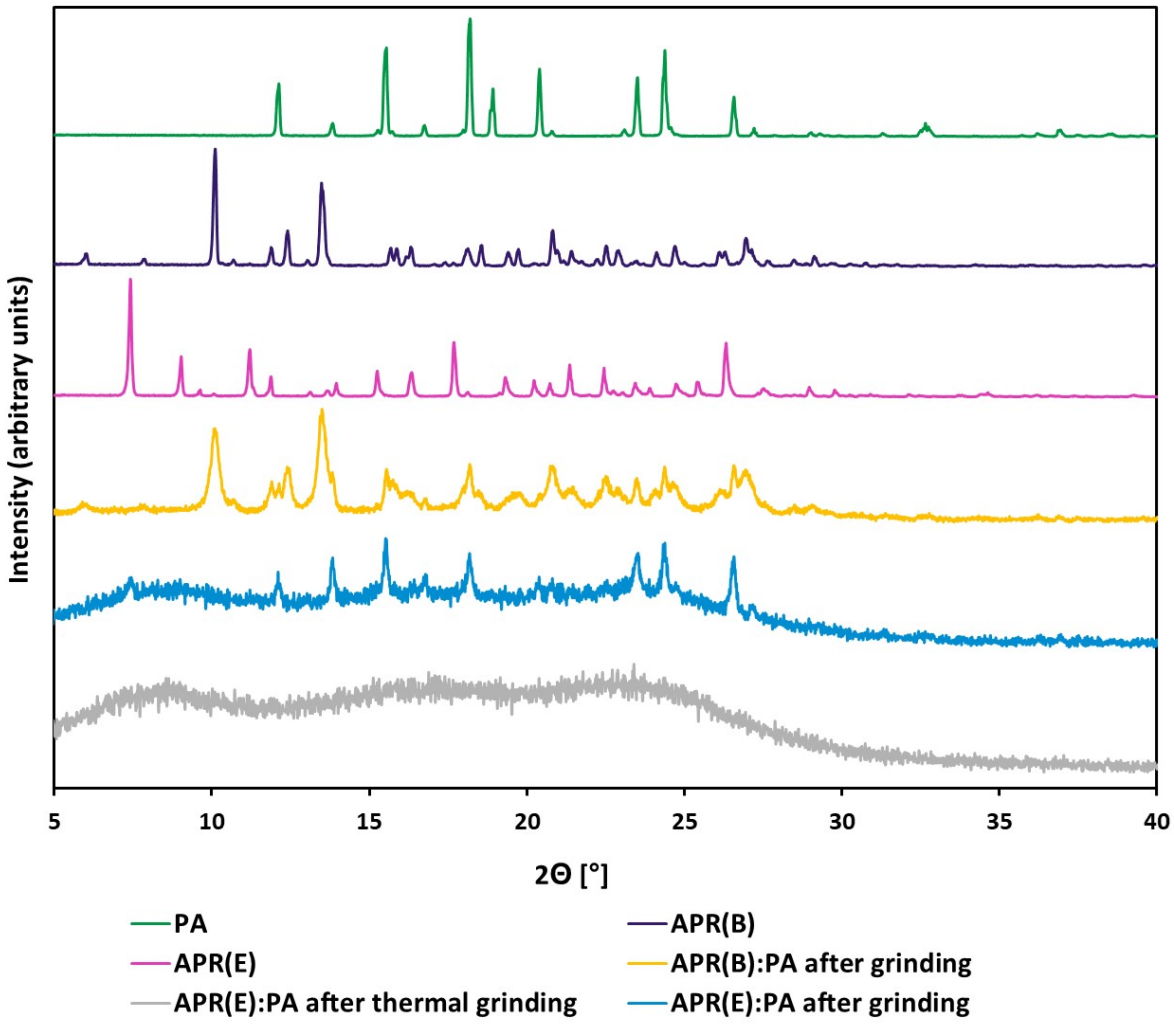

Figure S3c. Normalised PXRD patterns of pure PA, APR(B), APR(E), and APR:PA after grinding.

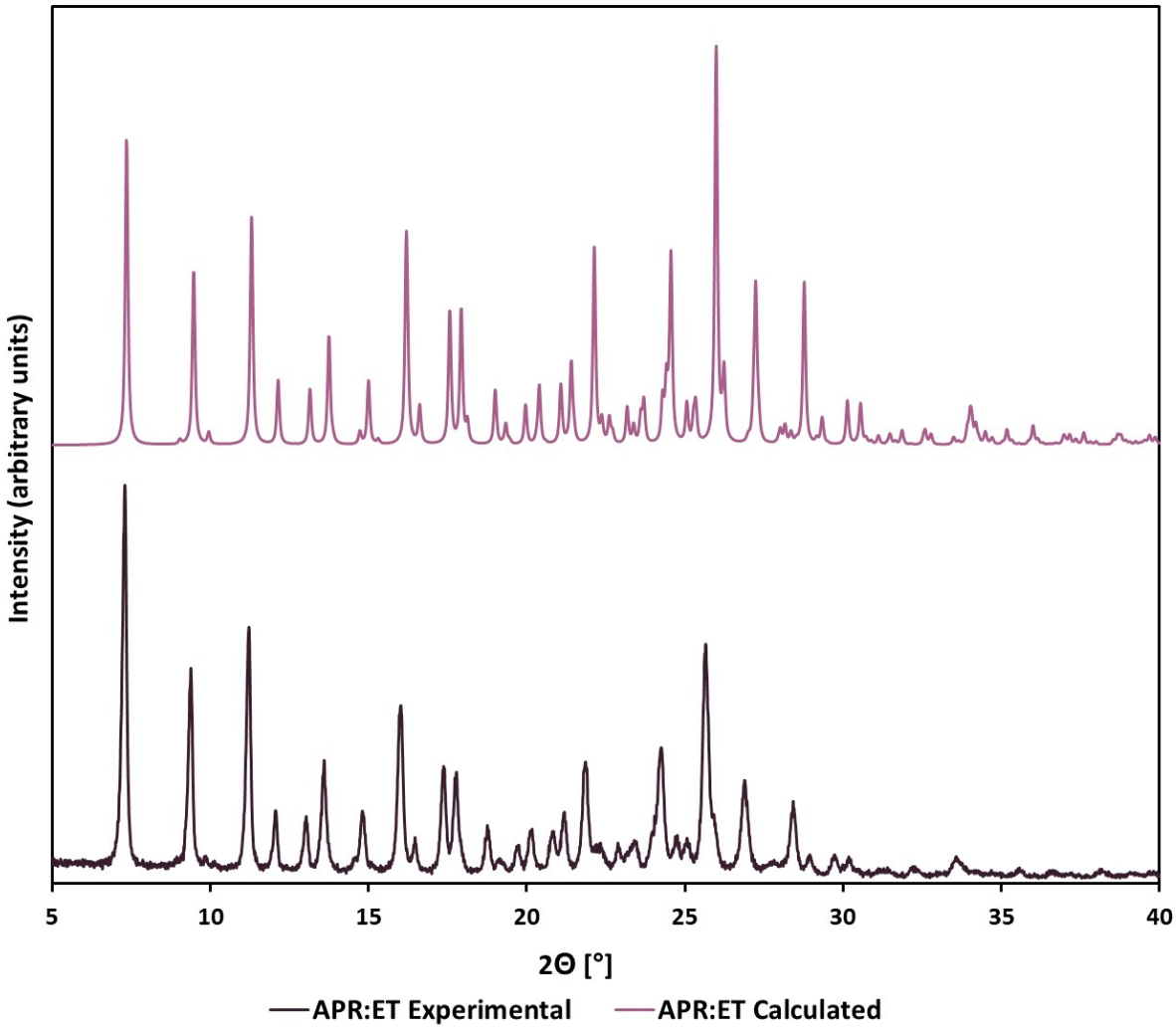

Figure S3d. Experimental and calculated PXRD patterns of the APR:ET cocrystal.

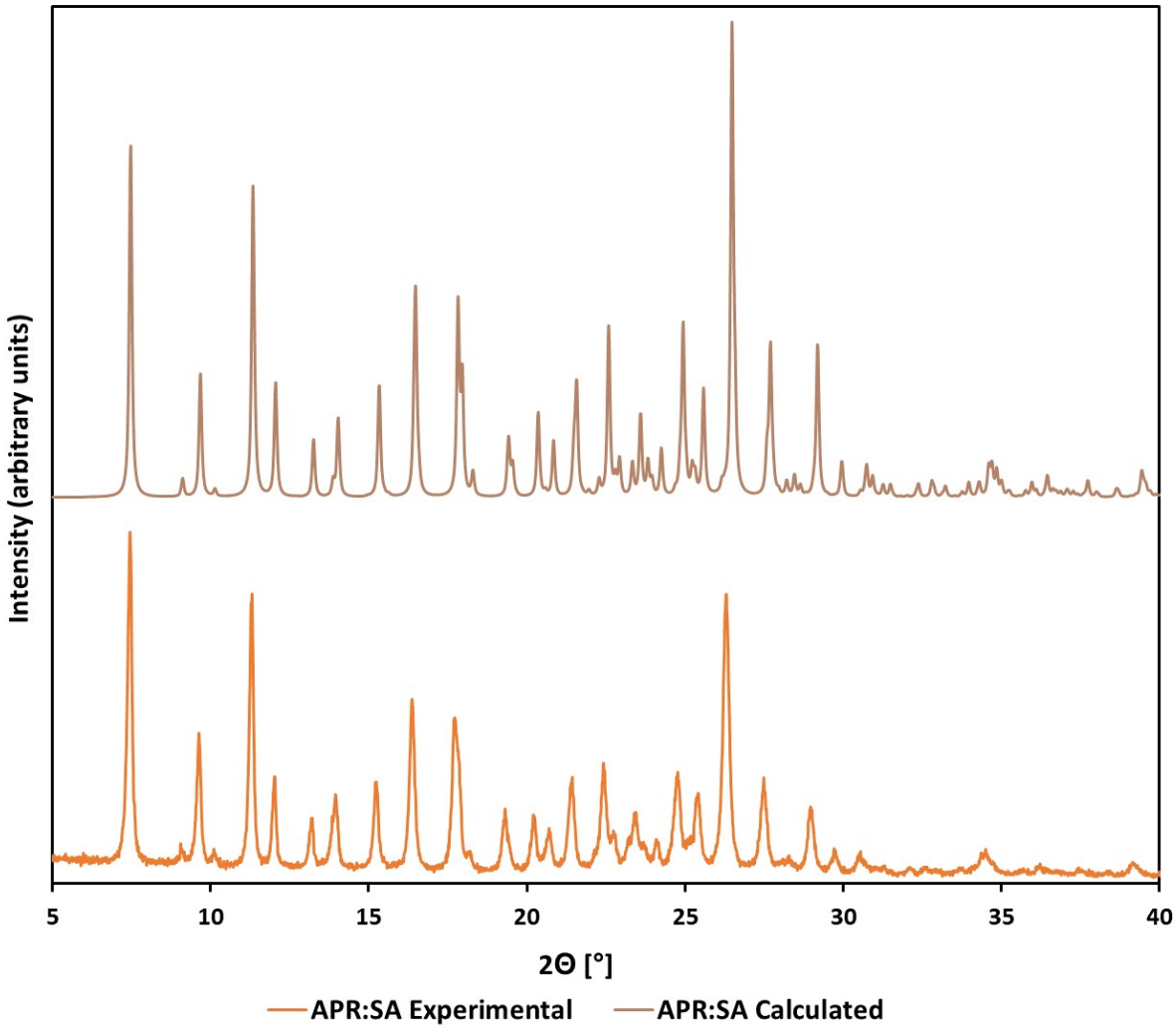

Figure S3e. Experimental and calculated PXRD patterns of the APR:SA cocrystal.

4) Arguments for treating the binary APR:PA system as a coamorphic sample

Distinguishing between a physical mixture of amorphous components and a co-amorphous system is not trivial. There is no single universal technique that would provide a definitive answer. Below, we present the arguments that led us to propose the hypothesis that the object under study is a coamorphous system. Our conclusions are based on our own experiences with paracetamol research and literature reports.

From the works cited in the manuscript (e. g. doi:10.1016/j.ejps.2007.04.002) and our studies using solid-state NMR spectroscopy, it follows that the lifetime of the sample in the amorphous glassy state is very short, and a sample subjected to thermal processes readily transitions from the molten state to the crystalline form, forming polymorph I, polymorph II, or polymorph III, or a mixture of them.(Mol. Pharmaceutics 2014, 11, 1326−1334, doi.org/10.1021/mp400768m, European Journal of Pharmaceutics and Biopharmaceutics 69 (2008) 364–371, doi:10.1016/j.ejpb.2007.10.008).

The final effect, which polymorph form of PA will dominate, is difficult to control and strongly depends on the cooling temperature gradient. The Figure S4 shows ^{13}C CP/MAS NMR spectra of paracetamol with different solid-state phase organization.

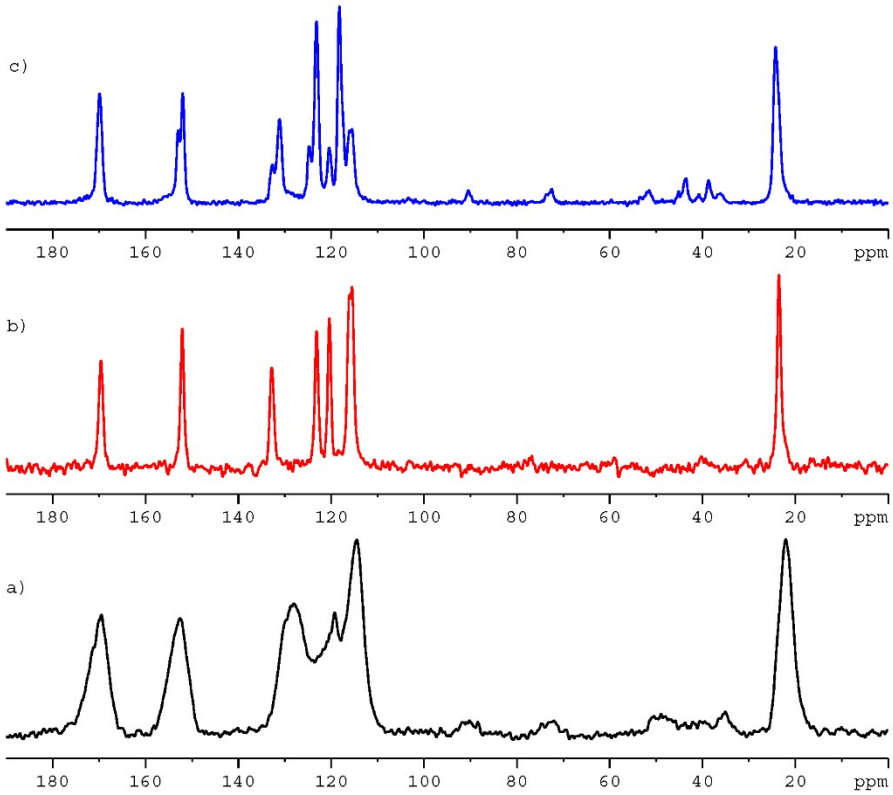

Figure S4. ^{13}C CP/MAS spectra of paracetamol sample a) after melting at temp 190°C. b) spectrum of polymorph I c) spectrum of mixture of polymorphs I and III.

Figure S4a shows paracetamol in an amorphous glassy state. This spectrum is characterized by very broad lines. In this state of matter, the sample is metastable and undergoes a phase transition to the crystalline form, forming polymorph I (Figure S4b). When the sample in the amorphous glassy state is slowly cooled at a rate of 30°C per hour, a mixture of polymorphs I and III is obtained (Figure S4c). It is worth noting that during thermomechanical milling of paracetamol polymorph I at a temperature of 160°C, no formation of other forms was observed. The excellent structure of polymorph I was preserved.

Figure S5 show a sample of APR:PA obtained by thermomechanical milling of two crystalline components at 160°C. Analysis of the spectra indicates that both coformers in the binary system are amorphous, and both spectra shown in Figure S4d and Figure S4e are very similar. The difference between S5a and S5b is that the first spectrum was recorded shortly after the preparation of the binary system (Figure S5a), whereas the same sample was recorded three months later, as shown in Figure S5b.

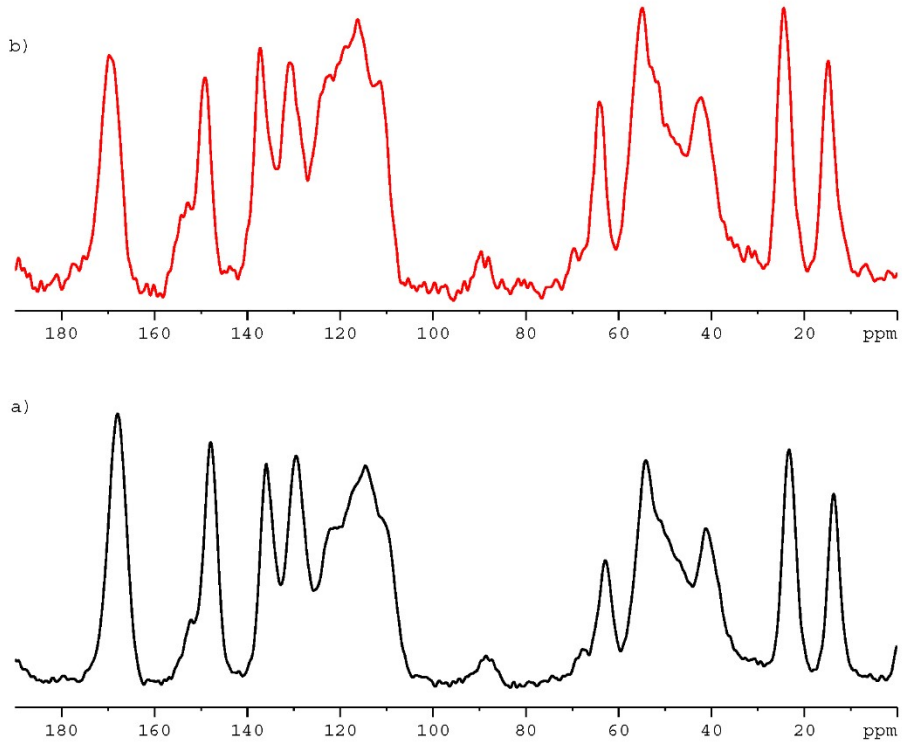

Figure S5. ^{13}C CP/MAS spectra of APR:PA binary system obtained by by thermomechanical milling of two crystalline components at 160°C a) shortly after the preparation of the binary system b) sample recorded three months later.

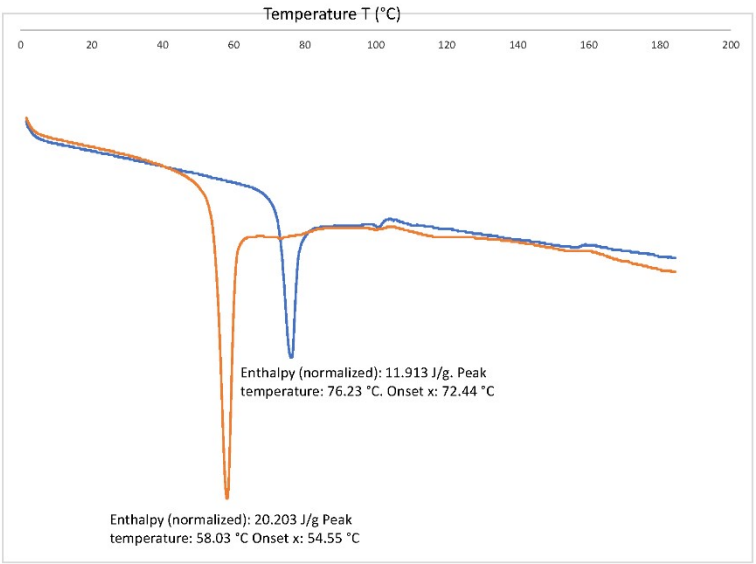

Figure S6. Differential Scanning Calorimetry (DSC) profiles showing glass transition temperature for amorphous samples a) orange line shows APR:PA obtained by thermomechanical milling b) blue line APR obtained by melting. The peak temperatures are 58.03 °C and 76.23 °C, respectively.

Figure 6 shows the DSC (differential scanning calorimetry) curves for the APR:PA mixture (orange line) and APR (orange line). The glass transition temperature (Tg) of pure amorphous apremilast is 76.23 °C. The curve for the APR:PA mixture shows only one Tg, which is a strong preliminary indication that the

sample has a homogeneous amorphous phase. This suggests that both components are intimately mixed at the molecular level and are not separated into domains of pure amorphous apremilast and pure paracetamol. Pure amorphous paracetamol usually has a glass transition temperature (Tg) of around 23-25 °C, although this can vary depending on the preparation method and measurement conditions. The Tg of the APR:PA mixture (58 °C) lies between the Tg of pure amorphous paracetamol (~24°C) and pure amorphous apremilast (76°C). This intermediate Tg value is exactly what is predicted by the Gordon-Taylor equation or similar models for a homogeneously mixed, single-phase amorphous system. The fact that it is not 76°C (pure apremilast) proves that apremilast is no longer in a pure amorphous state and has been plasticized by the presence of paracetamol. Finally, we measured the ^{1}H T_1 relaxation times using indirect detection of ^{13}C signals in two-dimensional (2D) mode for the amorphous APR sample and the coamorphous APR:PA. In both cases, the relaxation times were calculated using monoexponential functions, which means that in both cases the solid phase is homogeneous. In the case of heterogeneous phases, a biexponential function (or even a more complex one) should be used to fit the T_1 values. It is worth noting that for both samples, the ^{1}H T_1 values are relatively short, around 2 s, with a small dispersion of ^{1}H T_1 values. On the other hand, ^{1}H T_1 for crystalline PA is extremely long, amounting to 445 s for the aromatic residue and 38 s for the methyl group.

The above results allow for two conclusions. First, paracetamol can undergo permanent amorphization in the presence of apremilast, which is not observed for PA in its pure form. Second, the amorphous state of paracetamol in the binary system is stable, and the tendency to regain the crystalline structure of PA is suppressed. This means that both components work together at the molecular level, which is one of the criteria, although not a decisive one, for classifying a sample as a coamorphous system.

5) DSC curves for APR(B), APR(E), SA, ET, PA and binary systems APR:SA, APR:ET, and APR:PA.

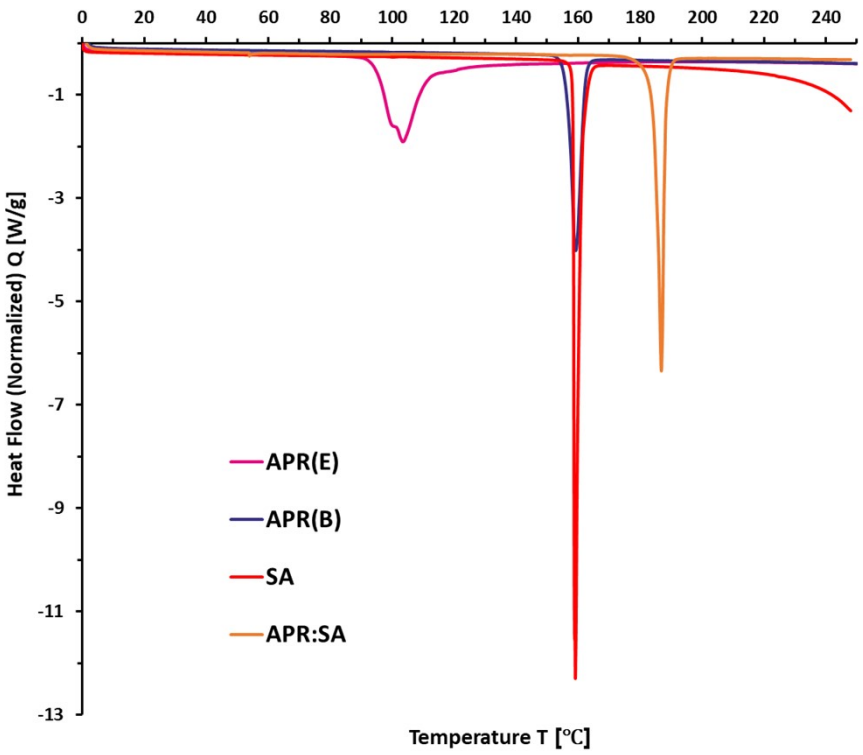

Figure S7a. DSC thermograms of the pure compounds (APR, SA) and APR:SA cocrystal.

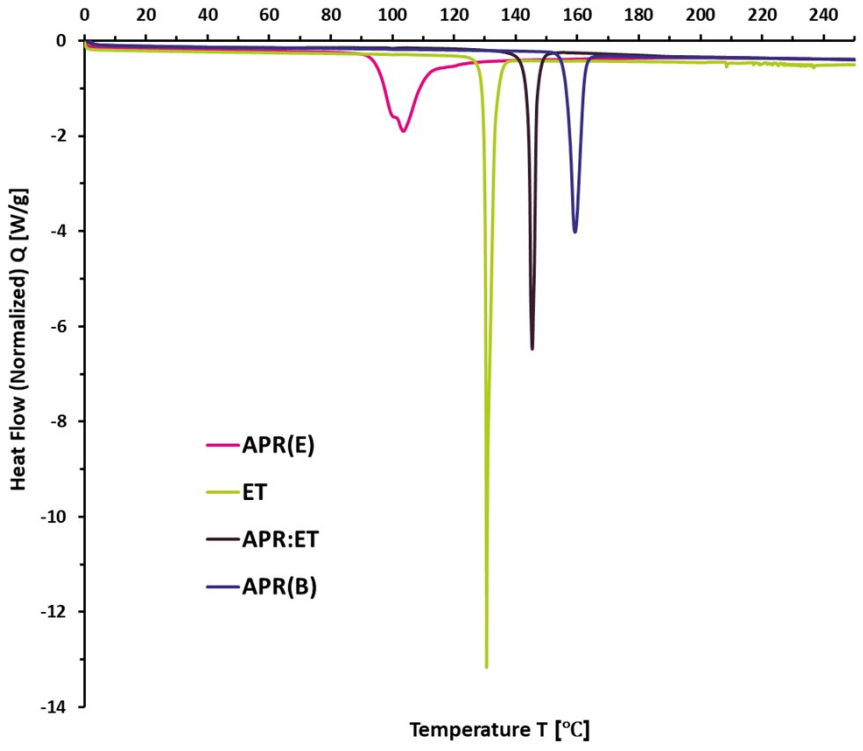

Figure S7b. DSC thermograms of the pure compounds (APR, ET) and APR:ET cocrystal.

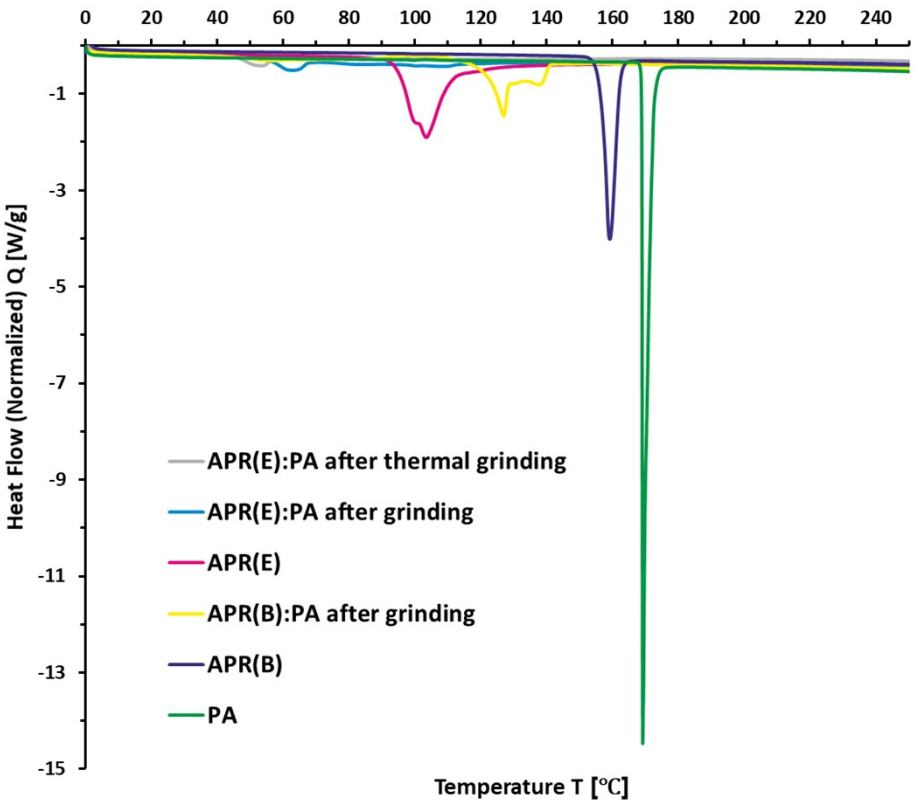

Figure S7c. DSC thermograms of the pure compounds (APR, PA) and APR:PA binary systems after grinding.

6) Experimental data for single crystal X-ray analysis of APR:ET.

Table S1. Experimental details.

Compound	**Apremilast: ethenzamide**
Crystal data	
CCDC	2513155
Chemical formula	$4(C_{22}H24N2O7S) \cdot 2(C_9H_{11}NO)$
Formula weight	2172.34
Crystal system	tetragonal
Space group	$P4_12_12$
Temperature (K)	100.00(10)
a [Å]	13.1968(1)
b [Å]	13.1968(1)
c [Å]	29.1386(3)
	90
β [°]	90
	90
V [Å^3]	5074.65(9)
Z	2
Z’	1
d_{calc} [g/cm^3]	1.422
Crystal dimensions [mm]	$0.15 \times 0.15 \times 0.10$
Radiation type	CuKα
μ [mm^{-1}]	1.614
Data collection	
Reflections measured	50488
Range/indices (*h*, *k*, *l*)	-16, 16; -12, 16; -36, 36
θ (max, min) [°]	80.270, 3.677
Total no. of unique data	5495
No. of observed data, I > 2σ(I)	5341
R_{int}	0.076
Refinement	
R [$F^2 > 2\sigma(F^2)$]	0.044
$wR(F^2)$	0.098
S	1.068
No. of reflections	5495
No. of parameters	426
No. of restraints	141
H-atom treatment	H atoms treated by a mixture of independent and constrained refinement
Δρ (min, max), e/Å^3	-0.28, 0.44

7) Modeling of the NMR chemical shifts

Structures of SA; ET; the polymorph E of APR; cocrystal formed by SA and the polymorph E of apremilast (APR:SA); and cocrystal formed by ET and the polymorph E of APR (APR:ET) were considered. Both the periodic and cluster models were applied. The modeling was performed in three consecutive steps.

In the first step, the periodic DFT computations were performed using the PBE functional to optimize the SA and ET crystal structures. For these optimized structures, the NMR chemical shielding, σ, was predicted by the GIPAW-PBE method. An excellent agreement between the ^{13}C σ data and measured ^{13}C chemical shifts, δ, was found. Specifically, for a linear fit of σ to δ, the root mean square deviation (RMSD) of only 0.8 and 1.2 ppm was obtained for the carbon nuclei of SA and ET, respectively.

In the second step, the periodic structures were employed to create a hydrogen-bonded dimer of SA and a hydrogen-bonded tetramer of ET. The NMR chemical shielding in these clusters was predicted by the GIAO-B3LYP/6-311++G(2d,2p) approach. The level of agreement between theory and experiment was found to be good, with the aforementioned RMSD now amounting to 1.4 and 2.2 ppm for the carbons of SA and ET, respectively. Hence, these clusters were used for a conversion of the computed ^{13}C chemical shielding to the ^{13}C theoretical chemical shifts, ε. Namely, $\epsilon = -0.8651 \times \sigma + 170.7$ ppm for the SA model, and $\epsilon = -0.9622 \times \sigma + 175.3$ ppm for the ET model.

In the third step, the periodic structure of APR, without acetonitrile molecules, was optimized using the PBE functional. A dimer of APR molecules was clipped out of this structure to approximate the pocket present in APR:SA and APR:ET cocrystals (it should be noted that acetonitrile, SA and ET molecules are disordered in the $P4_12_12$ space group, which was used to solve APR, APR:SA and APR:SA crystal structures, and hence it was not feasible to perform the periodic computations in the CASTEP program). Into this pocket, SA and ET molecules were docked to model the respective cocrystals. The GIAO-B3LYP/6-311++G(2d,2p) chemical shielding was obtained for these models and converted to the ^{13}C theoretical chemical shifts using the expressions shown above. In particular, the predicted chemical shifts of the carbonyl carbon in SA and APR:SA are 175.2 and 170.2 ppm, respectively. They agree well with the measured values of ca. 175.6 and 170.9 ppm. The predicted chemical shifts of the phenolic carbon in SA and APR:SA are 163.1 and 161.6 ppm, respectively. Their experimental counterparts amount to ca. 161.7 and 161.8 ppm and an agreement between theory and measurements is satisfactory. Moreover, the predicted chemical shifts of the carbonyl carbon in ET and APR:ET are 173.3 and 170.2 ppm, respectively. Thus, they are in a qualitative agreement with the experimental values of ca. 173.5 and 165 ppm. In this way, the trends in the ^{13}C chemical shift changes have been confirmed.

8) Biological Studies

a) Preparation of compound solutions

Solutions of compounds: APR, ET, and the APR:ET cocrystal were prepared at a concentration of 0.25 mM. The prepared solutions were subjected to threefold serial dilutions in DMSO. The final concentration in the biological system was prepared by dissolving the DMSO compound solution in the growth medium to achieve an initial concentration of 250 nM (0.1% v/v DMSO).

b) Mammalian cell and Bacterial strains culture

The mouse embryonic fibroblasts NIH/3T3 was purchased from the American Type Culture Collection. Cells were cultured in Dulbecco's Modified Eagle's Medium (DMEM) supplemented with 10% of Fetal Bovine Serum (FBS) and 1% antibiotics (penicillin and streptomycin). The culture was maintained in an incubator at 37°C containing 5% CO_2.

Staphylococcus aureus (ATCC 25923), *Pseudomonas aeruginosa* (ATCC 27853), *Staphylococcus epidermidis* (ATCC 14990), and *Escherichia coli* (ATCC 25922) were obtained from LGC Standards (Teddington, UK). *S. aureus, P. aeruginosa, and S. epidermidis* were cultured on tryptic soy agar (TSA; Biomaxima, Lublin, Poland) and *E. coli* on Luria-Bertani agar (LB; Biomaxima, Lublin, Poland), in standard conditions (37°C, 24h) in a bacteriological incubator (Memmert). To prepare a bacterial suspension (0.5 on the McFarland scale), single bacterial colonies were added to sterile saline solution. The suspensions prepared in this manner were used in subsequent experiments.

c) Mammalian Cell viability assay

NIH/3T3 cells suspension with a concentration of 4×10^4 cells/mL were seeded into 96-well plates and allowed to adhere for 24 h under standard culture conditions. Then, the compounds diluted in culture medium were added to the cells, resulting in a final DMSO concentration of 0.1% (v/v). Following 24 h and 72 h compound exposure, the brightfield pictures of cell culture were recorded with help of ZEISS Axiovert 10 microscope equipped with 10x objective. Simultaneously, cell viability was assessed using the MTT assay to evaluate both the short-term and long-term cellular responses to the tested substances. The medium was removed and 50 µl of MTT solution (0.25 mg/mL) was added to each well and cells were incubated for 3 h. Subsequently, 200 µL of isopropanol was added to each well to solubilize the formazan product. Absorbance of formazan solution was measured at 570 nm with the help of a multiplate absorbance reader (Multiskan SkyHigh TC MD, ThermoFisher Scientific, Waltham, MA, USA).

d) Minimal inhibitory and bactericidal concentration

To evaluate the minimal inhibitory and bactericidal concentrations (MIC and MBC, respectively), 150 µL of the tested substances solution (APR, ET and APR:ET cocrystal, DMSO 0.1% v/v) was added to the first wells; 100 µL of Mueller-Hinton broth (Biomaxima, Lublin, Poland) was added to each well, and then 50 µL from the first well was transferred to create 3-fold dilutions of the tested substances. After

preparation of the tested substances, 10 µL of bacterial suspension was added to each well, including a positive control (medium without the tested substances) and a negative control (medium with DMSO without any microorganisms). Prepared plates were incubated at 37°C for 24 h. After incubation, the growth in each well was evaluated. Suspension from each well was placed in Mueller-Hinton agar plates in order to determine the minimal bactericidal concentration, and the plates were incubated in standard conditions (37°C, 24 h). Thereafter, the growth on the agar was evaluated.

e)Bacteria viability assay

To determine the viability of the cells, a PrestoBlue assay (ThermoFischer, Waltham, MA, USA) was performed. For this purpose, 10 µL of PrestoBlue reagent was added to each well of 96-well plates (containing medium with bacterial substances and tested substances in appropriate or control wells concentrations as described above). After incubation for 30 min (37°C without light), the fluorescence was measured at the wavelength of 560/590 nm.

f) Statistical analysis

Statistical analysis of the NIH/3T3 cells results was performed using GraphPad Prism software (version 9.2.0, San Diego, CA, USA). The results were expressed as % viability calculated by:

$$\frac{\textit{the average value of fluorescence from the test sample – the average value of the negative control}}{\textit{the value of the positive control – the average value of the negative control}}$$

The normality of data distribution was evaluated using the Shapiro-Wilk test. As the data did not demonstrate a normal distribution, the non-parametric Kruskal-Wallis test was employed. To compare all experimental groups with each other, Dunn's multiple comparisons post-hoc test was applied. The results from the bacterial viability assay were evaluated by one-way ANOVA with Tukey post hoc. A ρ-value of less than 0.05 ($\rho < 0.05$) was considered statistically significant.

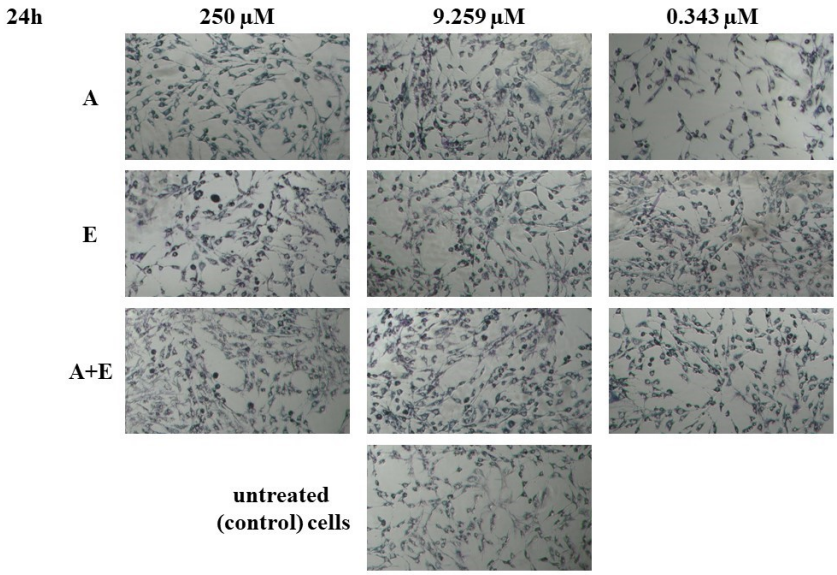

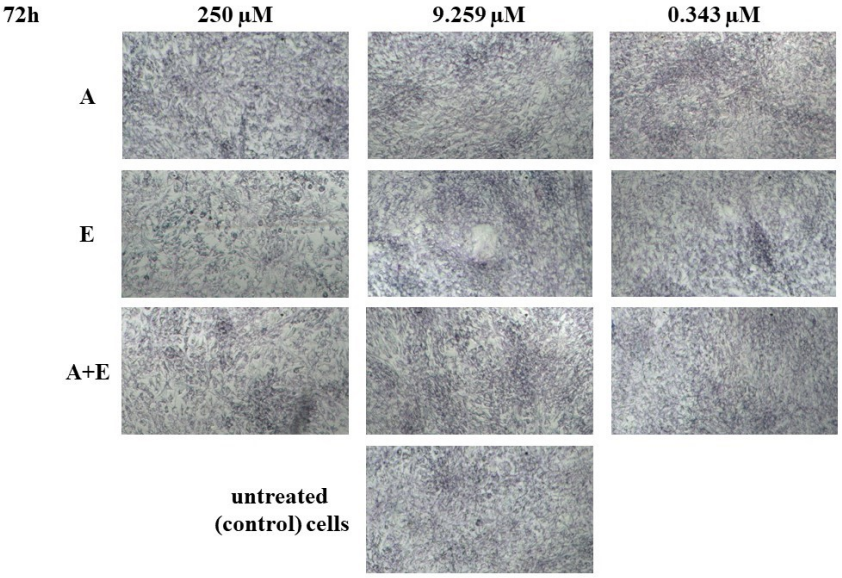

Figure S8a. Brightfield microscopic images of the NIH3T3 cell culture after a) 24 h and b) 72 h of incubation with the studied compounds.

S. aureus

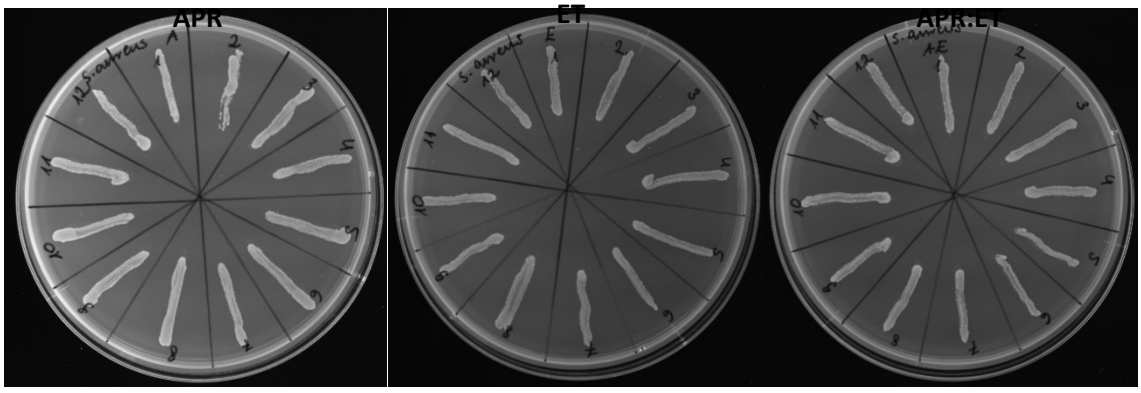

P. aeruginosa

S. epidermidis

E. coli

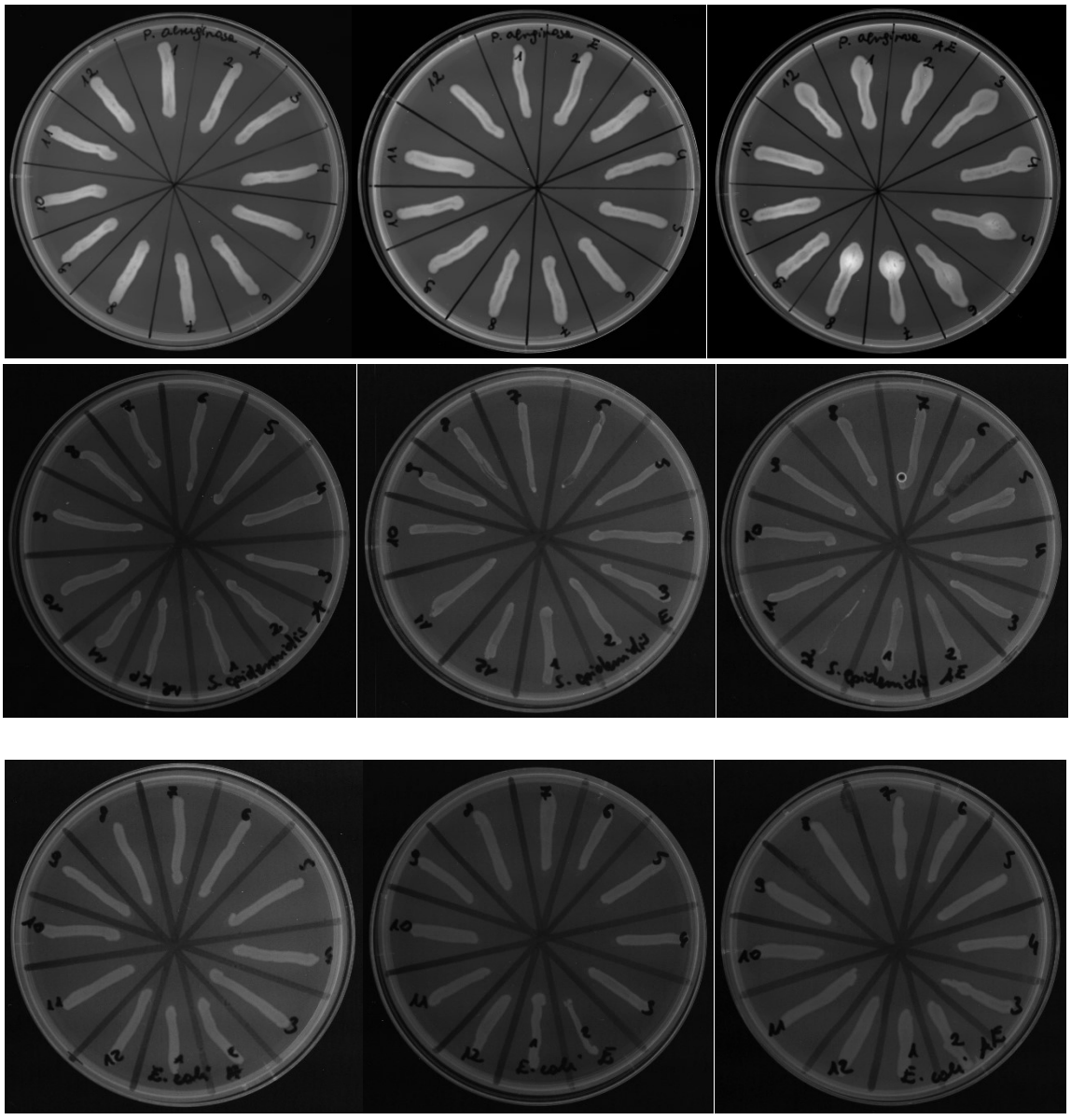

Figure S8b. Exemplary growth of microorganisms treated with substances tested in different concentrations. Numbers 1-11 indicate successive concentrations (triplicate); the field marked 12 is a positive control (untreated microorganisms). Left column, APR, middle column ET and right column APR:ET cocrystal.

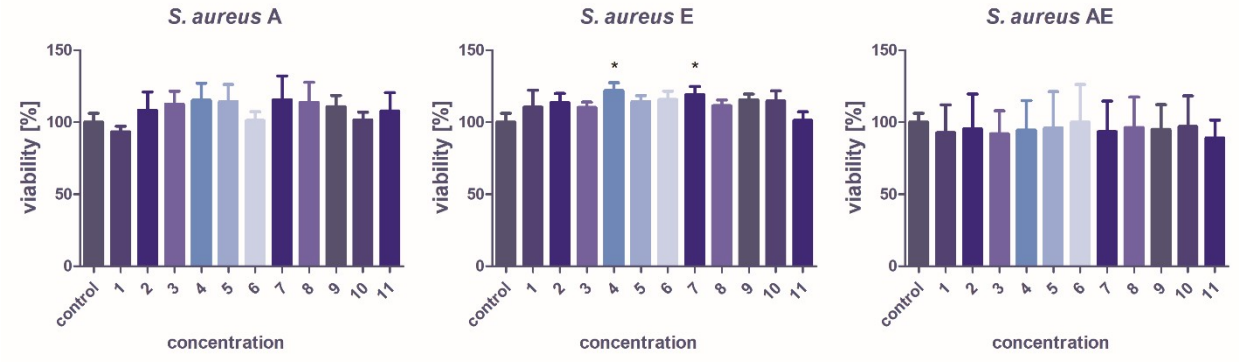

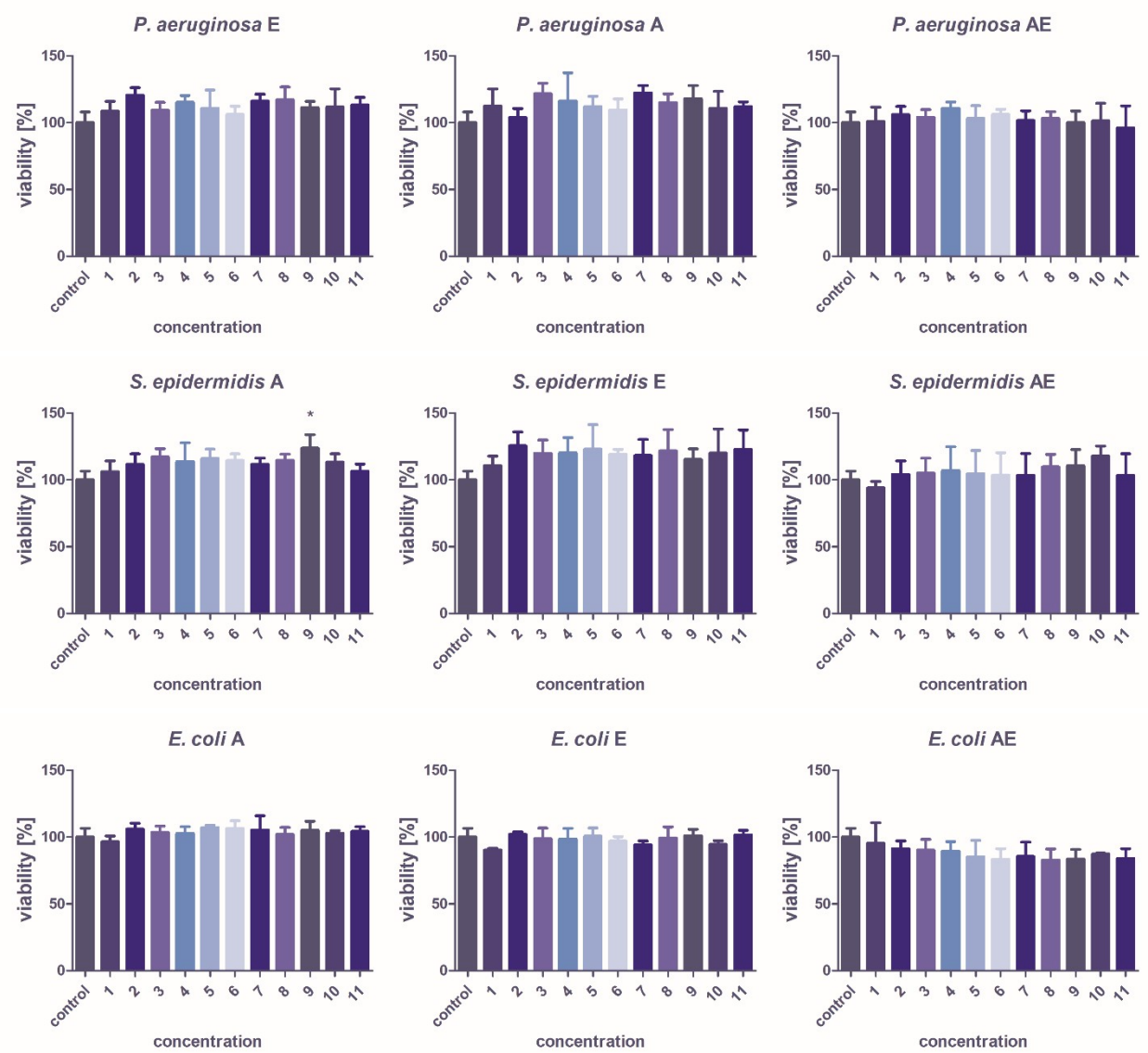

Figure S8c. Viability of *S. aureus, P. aeruginosa, E. coli,* and *S. epidermidis* treated with substances APR, ET, and APR:ET. Results are expressed as mean ± standard deviation. Numbers 1-11 indicate successive concentrations (triplicate). Statistically significant differences are marked with '*'. Control is a sample with a microorganism without treated substances.

Table S2 Minimal inhibitory and bactericidal concentrations of *S. aureus*, *P. aeruginosa*, *S. epidermidis* and *E. coli* treated with substances APR, ET and APR:ET cocrystal.

	S. aureus		*P. aeruginosa*		*S. epidermidis*		*E. coli*	
	MIC	MBC	MIC	MBC	MIC	MBC	MIC	MBC
APR	n.d.	n.d.	n.d.	n.d.	n.d.	n.d.	n.d.	n.d.
ET	n.d.	n.d.	n.d.	n.d.	n.d.	n.d.	n.d.	n.d.
APR + ET cocrystal	n.d.	n.d.	n.d.	n.d.	n.d.	n.d.	n.d.	n.d.

n.d. – not determined

9) Solubility Studies.

Table S3.

Sample	Concentration of APR in each sample [µg/ml]				Mean Concentration [µg/ml]	SD	RSD [%]
	pH 1.2						
APR(B)	11.37	10.23	10.12	10.15	**10.47**	**0.60**	5.78
APR(E)	121.60	128.80	122.10	129.20	**125.43**	**4.14**	3.30
APR(M)	166.28	163.73	163.70	160.70	**163.60**	**2.29**	1.40
APR:ET	16.05	16.94	17.04	17.84	**16.90**	**0.64**	3.76
APR:SA	5.83	4.42	4.70	4.47	**4.85**	**0.66**	16.32
APT:PA after thermal grinding	196.27	196.67	193.24	193.26	**194.86**	**1.87**	0.96
	pH 5.7						
APR(B)	8.38	9.59	9.24	9.88	**9.27**	**0.65**	7.01
APR(E)	101.25	101.94	111.35	102.24	**104.19**	**4.79**	4.59
APR(M)	132.30	128.47	129.71	126.15	**129.16**	**2.56**	1.98
APR:ET	14.82	16.78	14.72	15.47	**15.45**	**0.95**	6.13
APR:SA	37.01	41.38	42.42	37.52	**39.58**	**2.72**	6.86
APT:PA after thermal grinding	151.88	161.35	159.28	162.29	**158.70**	**4.72**	2.97
	pH 6.8						
APR(B)	9.02	8.05	8.41	9.45	**8.73**	**0.62**	7.13
APR(E)	99.33	96.18	103.37	100.81	**99.92**	**3.00**	3.00
APR(M)	125.04	124.08	122.61	122.30	**123.58**	**1.19**	0.97
APR:ET	13.46	13.99	14.60	15.38	**14.36**	**0.83**	5.76
APR:SA	38.65	42.64	40.40	44.40	**41.52**	**2.52**	6.07
APT:PA after thermal grinding	144.34	143.86	144.14	152.81	**146.29**	**4.35**	2.98

10) Theoretical calculations.

Table S4. The DFT-D (PBE/MBD*) total energies and its intra- and intermolecular contributions for the studied cocrystals. All values are expressed in kJ/mol of molecules.

crystal form	E^{total}	E^{inter}	E^{intra}	
HEBVET (APR:SA)	-873196	-294.40	-243008	SA
			-751397	APR
SALIAC20	-243123	-116.20	-243007	
ZOSXEN (APR_B)	-751626	-221.71	-751404	
delta	**-8.04**	**-14.59**	**6.55**	
APR:ET	-884456	-298.57	-265518	ET
			-751399	APR
DUKXAJ02	-265653	-158.49	-265495	
ZOSXEN (APR_B)	-751626	-221.71	-751404	
delta	**-3.57**	**2.39**	**-5.96**	
WUZLEL (APR:CIN)	-868735			
CINMAC07	-234228			
ZOSXEN (APR_B)	-751626			
delta	**4.79**			